Electronic Supplementary Information (ESI) for

Two tetranuclear Cd-based metal-organic frameworks for sensitive sensing of TNP/Fe^{3+} in aqueous medium and gas adsorption

Ruihong Guo[a], Lingling Gao[b], Jinxia Liang[a], Zhikai Zhang[a], Jie Zhang[a], Xiaoyan Niu[a], and Tuoping Hu[a*]

[a]Department of Chemistry, College of Science, North University of China, Taiyuan 030051, China
[b]College of Chemistry and Chemical Engineering, Jinzhong University, Taiyuan 030619, China

E-mail: hutuopingsx@126.com.

1. Materials and Methods. All solvents and reagents were commercially purchased and used directly. Thermogravimetric analyses (TGA) were measured on a ZCTA analyzer from ambient temperature to 800 ℃ at a raising rate of 10 ℃ min^{-1} under nitrogen flowing. Infrared (IR) spectra of the title MOFs were obtained from KBr pellets on a spectrometer of FTIR-8400S from 600 cm^{-1} to 4000 cm^{-1}. PXRD patterns of MOFs were measured on a diffractometer (Rigaku D/Max-2500 PC) with Cu-Kα radiation at ambient temperature (2θ = 5-50°). Elemental analyses (H, C, N) were perfromed by using a Vario MACRO analyzer. Luminescence experiments were carried out on a spectrophotometer (F-4600 FL) at room temperature. The sorption behaviors for different gases were assessed using ASAP-2020 analyzer.

2. X-ray crystallography. X-ray crystallography data for MOFs **1-2** were collected using a Bruker Apex Smart CCD diffractometer at 296 K (**1**) and 150 K (**2**) with graphite-monochromatized Mo-*Kα* radiation (λ = 0.71073 Å). Absorption corrections were carried out. The structures of MOFs were saved by direct methods using SHELXTL-2016 package with full-matrix least-squares methods on F^2. Crystal data and refinements for **1** and **2** were summarized in Table S4, and selected bond angles and separations were listed in Table S5 and S6. The CCDC numbers are 1956741 (**1**), 1956743 (**2**), respectively.

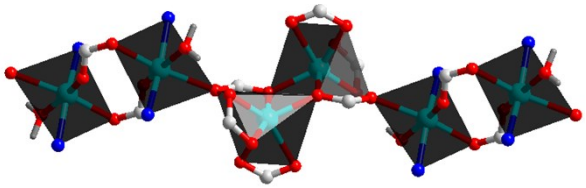

Fig. S1. The $\{Cd_4(COO)_8\}$ SBUs ($Cd^{II}1$ and $Cd^{II}2$) in **1**.

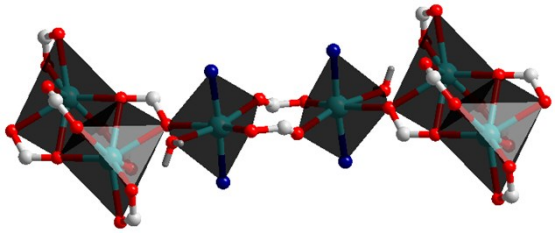

Fig. S2. The $\{Cd_4(COO)_8\}$ SBUs ($Cd^{II}3$ and $Cd^{II}4$) in **1**.

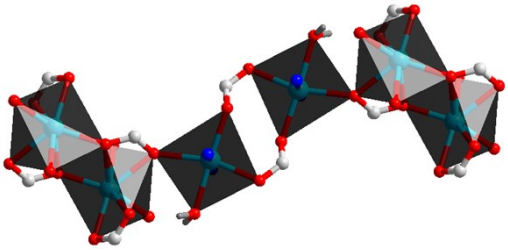

Fig. S3. The $\{Cd_4(COO)_8\}$ SBUs in **2**.

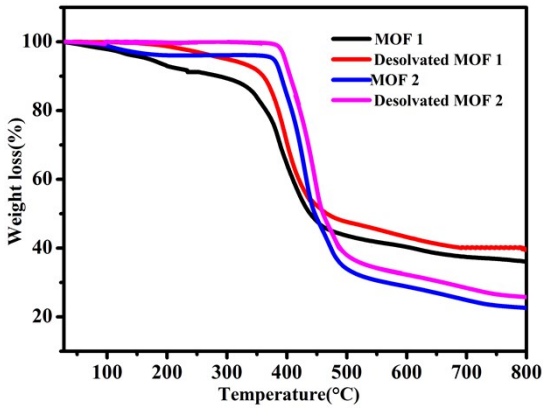

Fig. S4. TGA curves of Cd-MOFs and AMOFs.

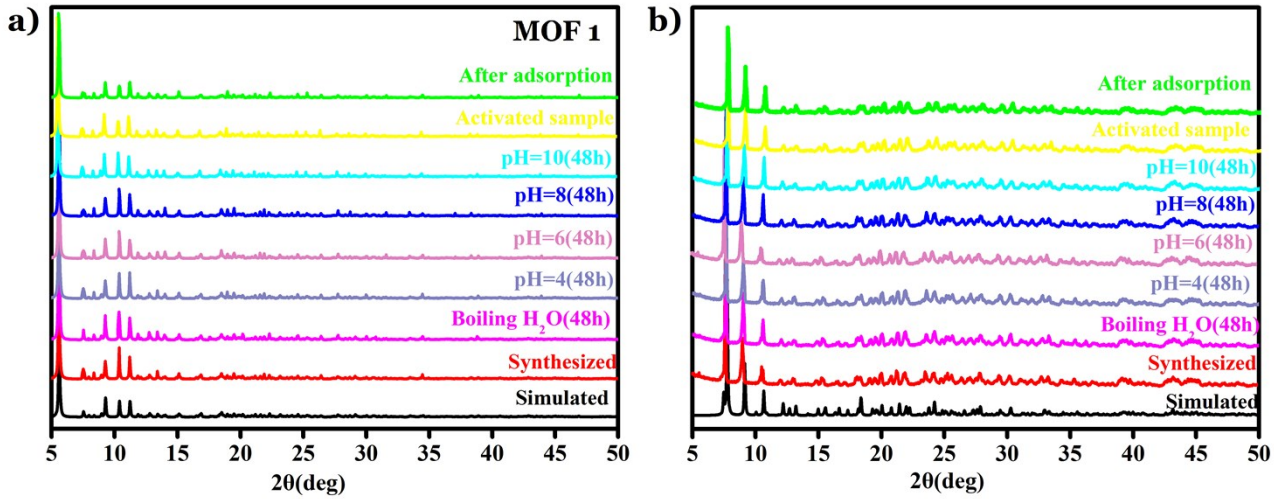

Fig. S5. PXRD patterns of MOFs **1** and **2** at different conditions.

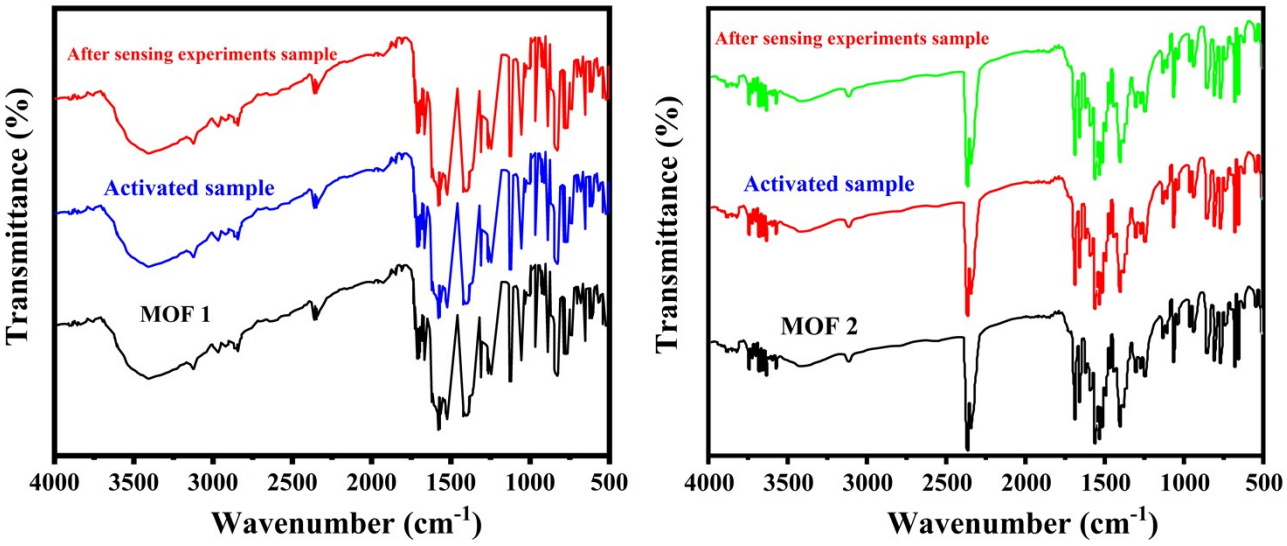

Fig. S6. The IR spectra of MOFs **1** and **2** at different conditions.

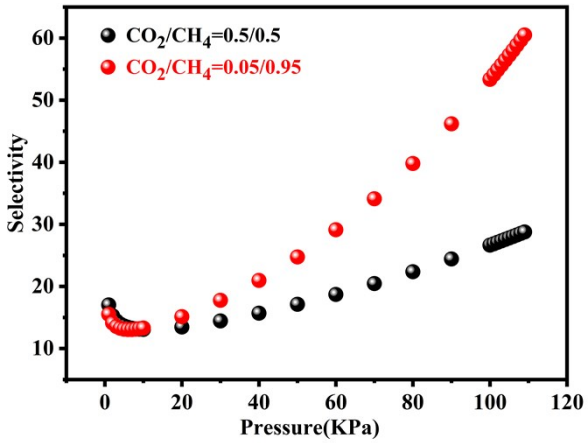

Fig. S7. Selectivity calculated by IAST of **1** at 298 K and 1 bar

CO_2/CH_4 Selectivity calculated by IAST

To compare the efficiency of MOF **1** for CO_2/CH_4 separation, the IAST of Myers and prausnitz along with the pure component isotherm fits were used to determine the molar loadings in the mixture for specified partial pressures in the bulk gas phase. The measured experimental data on pure component isotherms for CO_2 and CH_4 were first converted to absolute loading using the Peng-Robinson equation of the fluid densities. The absolute component loading at 298 K were fitted with a single-site Langmuir-Freundlich model (Equation 1).

$$N = a \times \frac{bp^c}{1 + bp^c} \quad (1)$$

(a is saturation capacity, b and c are constant)

The adsorption selectivities, Sads, for binary mixtures of CO_2/CH_4, defined by (Equation 2):

$$S_{ads} = \frac{x_i / x_j}{y_i / y_j} \quad (2)$$

(S_{ads}: adsorption selectivity; x_i: the mole fractions of component i in the adsorbed phases; y_i: the mole fractions of component i in the bulk phases.)

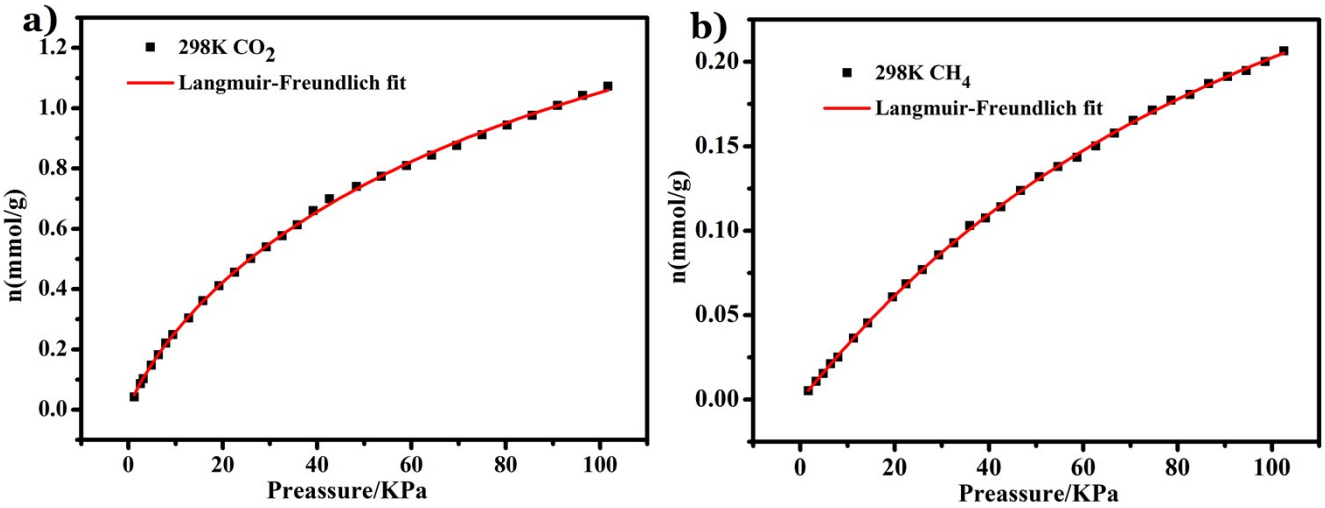

Fig. S8. (a) CO_2 adsorption isotherms of **1** at 298K with fitting by L-F model: a = 2.18297, b =0.01933, c = 0.84114, $Chi^2 = 4.42092\times10^{-4}$, $R^2 = 0.99949$; (b) CH_4 adsorption isotherms of **1** at 298K with fitting by L-F model: a = 0.43319, b = 0.00742, c = 1.03631, $Chi^2 = 1.45383\times10^{-4}$, $R^2 = 0.99977$.

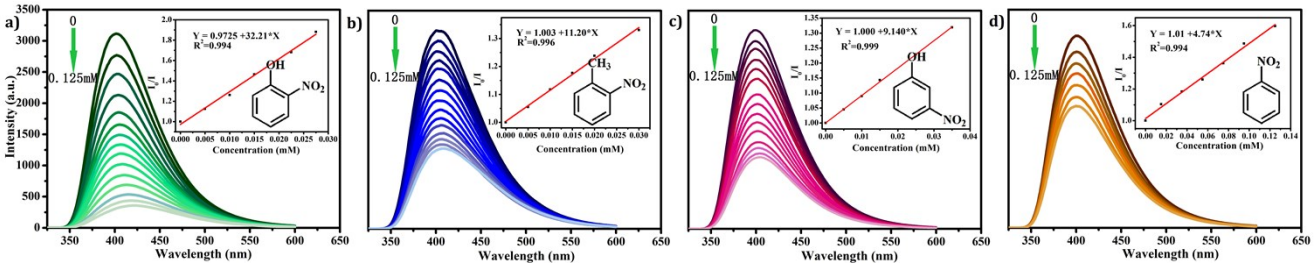

Fig. S9. The PL spectra of the **1**@H_2O suspension on incremental addition of o-NP(a), o-NT(b), m-NP(c) and NB(d). Inset: the SV plot

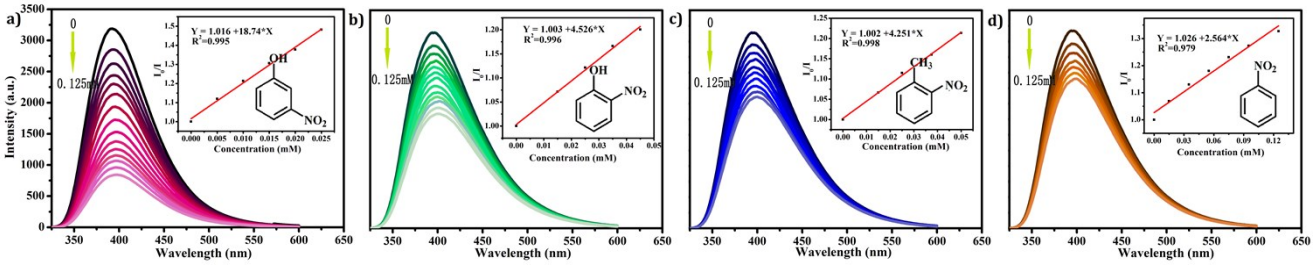

Fig. S10. The PL spectra of the **2**@H_2O suspension on incremental addition of m-NP(a), o-NP(b), o-NT(c) and NB(d). Inset: the SV plot

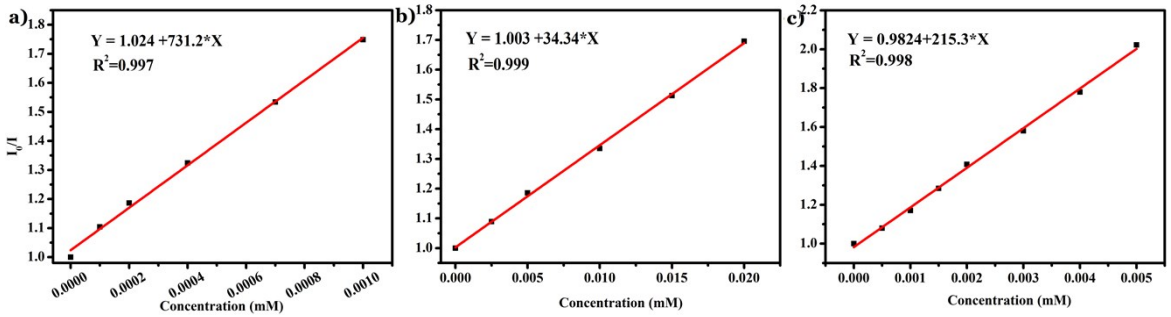

Fig. S11 The linear plots at low concentrations of TNP (a), PNP(b) and Fe^{3+} (c) for **1**.

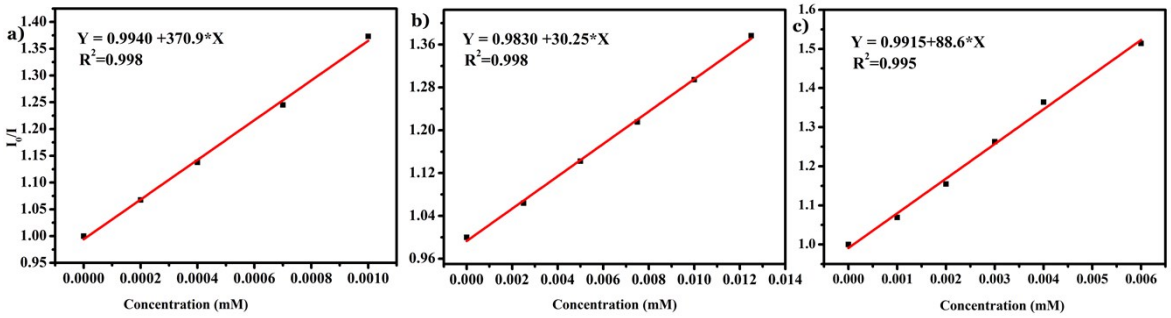

Fig. S12 The linear plots at low concentrations of TNP (a), PNP(b) and Fe^{3+} (c) for **2**.

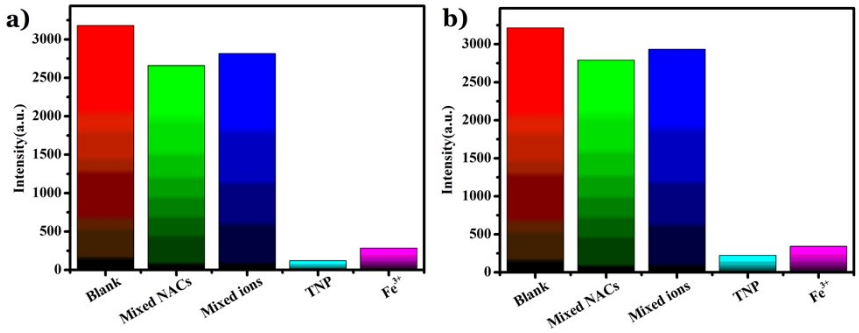

Fig. S13 The anti-interferences of **1**(a) and **2**(b) for sensing of TNP and Fe^{3+} from normal analytes in aqueous solution: blank, after addition of mixed NACs(PNP, m-NP, o-NP, o-NT, NB), after addition of mixed metal ions (Ag^+, K^+, Na^+, Ba^{2+}, Cd^{2+}, Zn^{2+}, Ca^{2+}, Cu^{2+}, Pb^{2+}, Co^{2+}, Hg^{2+}, Al^{3+}, Cr^{3+}), and followed by addition of TNP or Fe^{3+} ions, respectively.

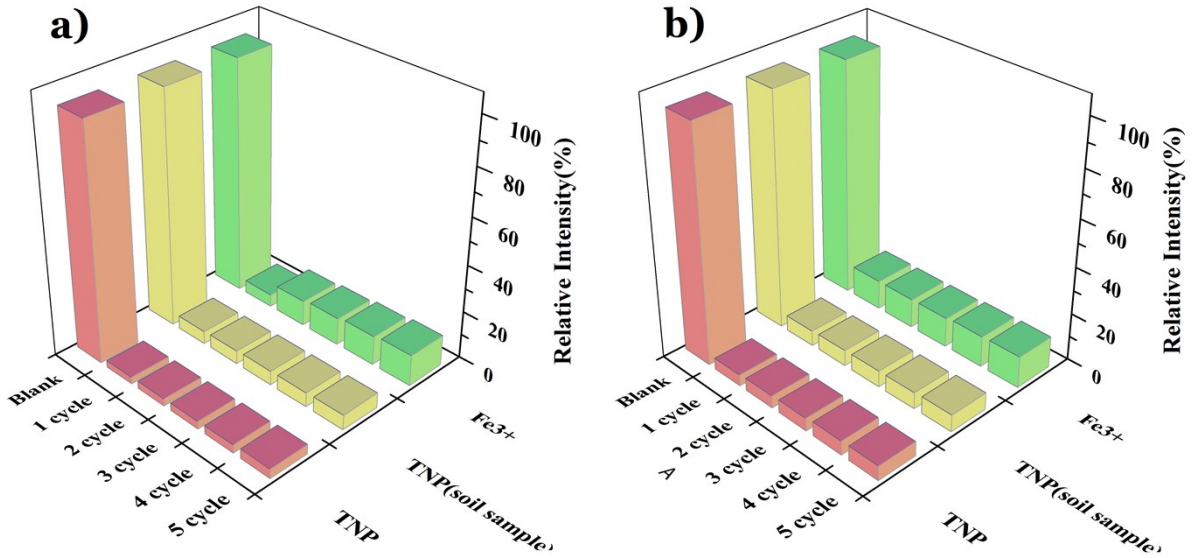

Fig. S14 Cycle tests of **1**(a) and **2**(b) for sensing TNP and Fe^{3+}.

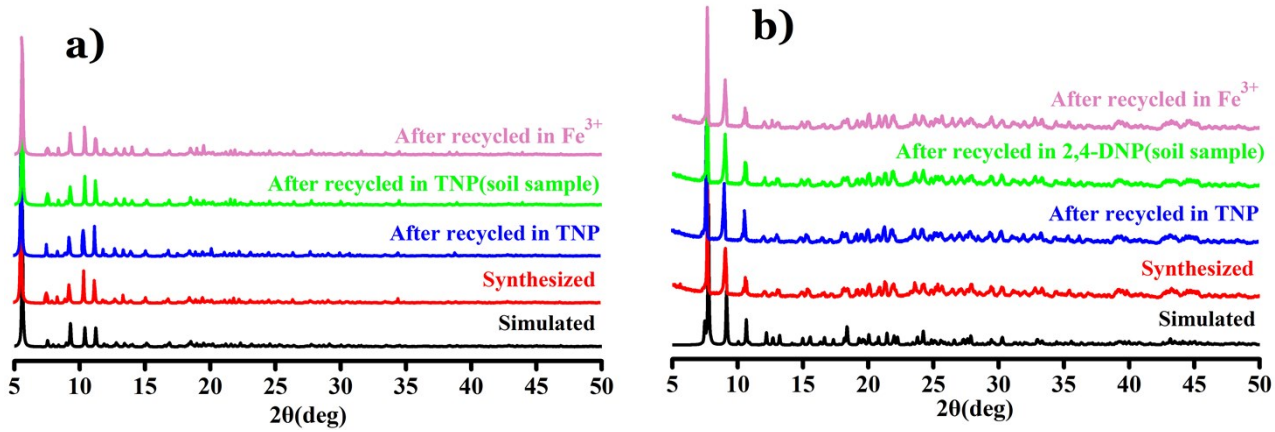

Fig. S15 The PXRD patterns of **1**(a) and **2**(b) after being immerged in the analytes.

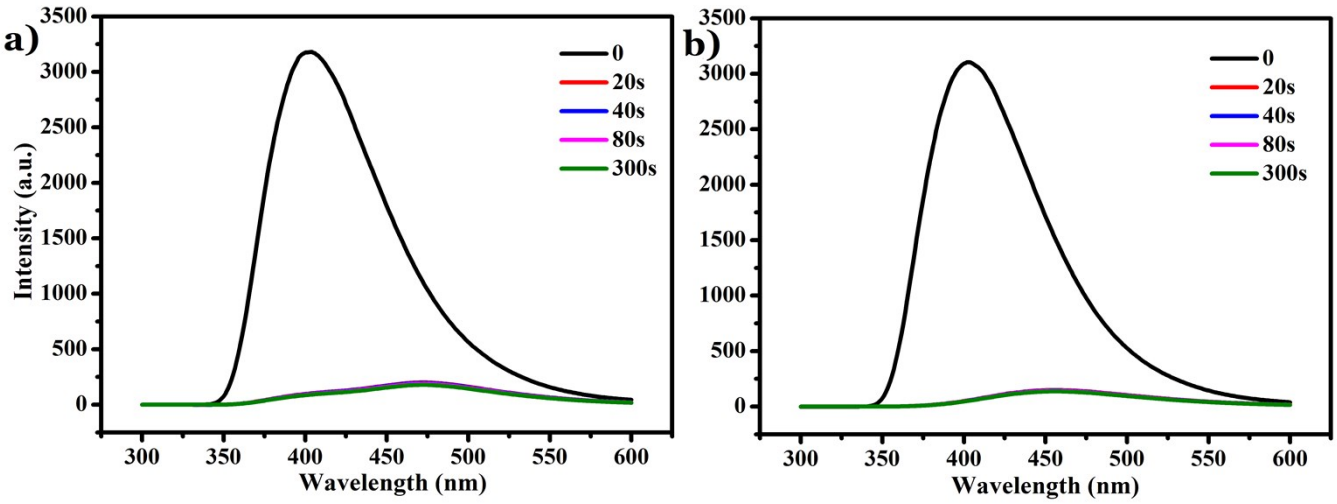

Fig. S16 The PL spectra of time-dependent after **1** immersed in 0.1 mM TNP(a) and Fe^{3+}(b) aqueous solution for different time.

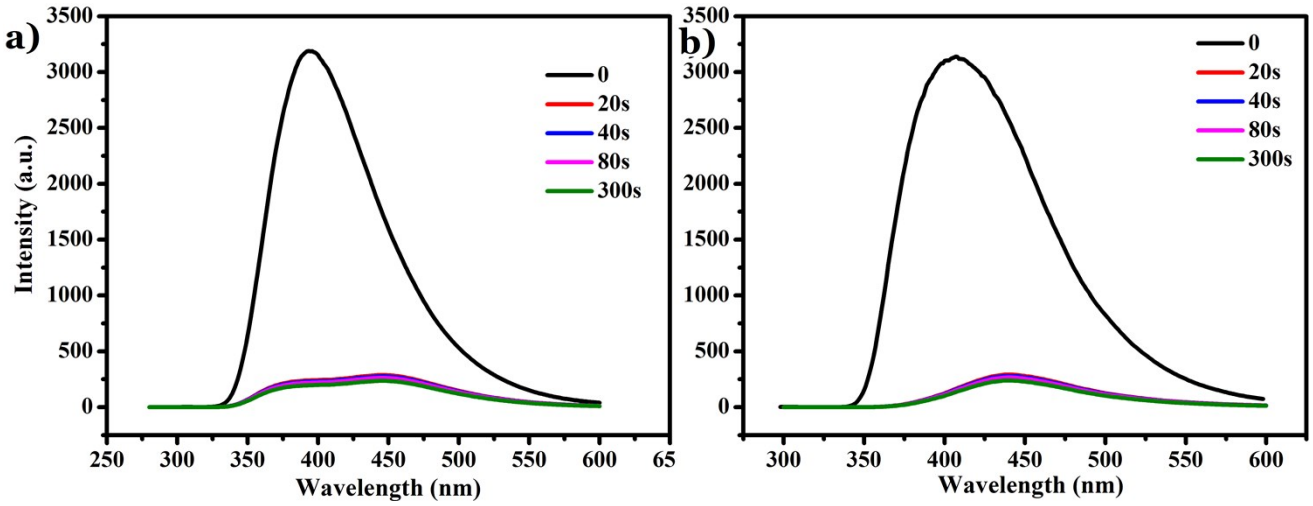

Fig. S17 The PL spectra of time-dependent after **2** immersed in 0.1 mM TNP (a) and Fe^{3+} (b) aqueous solution for different time.

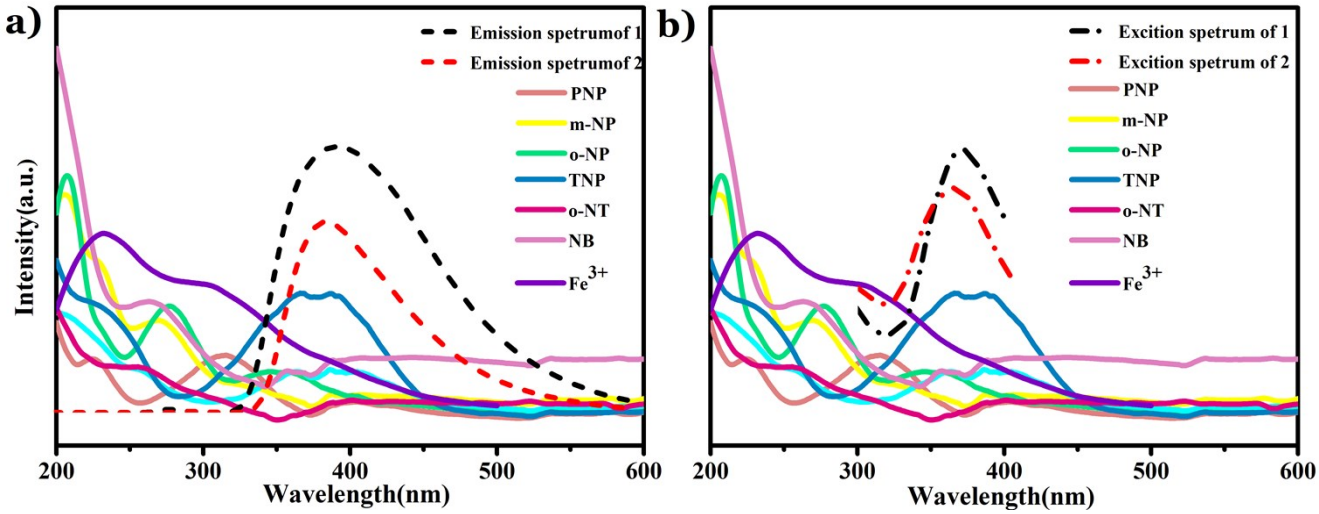

Fig. S18 Spectral overlap between the emission (a) and excitation (b) spectra of MOFs and the absorption spectra of NACs and Fe^{3+}.

Table S1. Comparison of the K_{sv} (M^{-1}) values of MOF **1**/**2** for sensing TNP in water with the previously reported MOFs' values

MOF sensor	K_{sv} (M^{-1})	Ref.
$\{[Cd_4(HDDCP)_2(4,4'\text{-bibp})_2(H_2O)_2]\cdot 2.5(DOA)\cdot 1.5(H_2O)\}_n$(**1**)	7.31×10^5	This work
$\{[Cd_2(HDDCP)(1,4\text{-bib})(H_2O)]\cdot H_2O\}_n$ (**2**)	3.71×10^5	This work
$[In_3O(ADBA)_3(H_2O)_3](NO_3)\cdot(H_2O)_6$	1.28×10^5	*J. Mater. Chem. A, 2018,* ***6****, 17177*
$[Zn_4(DMF)(Ur)_2(NDC)_4]$	1.08×10^5	*Cryst. Growth Des., 2015,* ***15****, 3493-3497*
$\{[Tb(L_1)_{1.5}(H_2O)]\cdot 3H_2O\}_n$	7.47×10^4	*J. Coord. Chem., 2018,* ***71****, 3994-4006*
$[Zn_2(NH_2BDC)_2(dpNDI)]_n$	7.3×10^4	*Chem. Eur. J., 2017,* ***23****, 16204-16212*
$\{[W_2(\mu_3\text{-}S)_6(\mu_4\text{-}S)_2Cu_8(CN)_4(3\text{-abpt})]\cdot CH_3CN\cdot H_2O\}_n$	6.36×10^4	*Inorg. Chem.2019,* ***58****, 9749-9755*
UiO-68@NH_2	5.80×10^4	*Cryst. Growth Des., 2015,* ***15****, 3493-3497*
$[Eu_3(bpydb)_3(HCOO)(\mu_3\text{-}OH)_2(H_2O)]$	2.1×10^4	*Adv. Funct. Mater. 2014,* ***24,*** *4034-4041.*

Table S2. Comparison of the K_{sv} (M^{-1}) values of MOF**1**/**2** for sensing Fe^{3+} in water with the previously reported MOFs' values

MOF sensor	K_{sv} (M^{-1})	Ref.
$\{[Cd_4(HDDCP)_2(4,4'\text{-bibp})_2(H_2O)_2]\cdot 2.5(DOA)\cdot 1.5(H_2O)\}_n$ (**1**)	2.15×10^5	This work
$\{[Cd_2(HDDCP)(1,4\text{-bib})(H_2O)]\cdot H_2O\}_n$ (**2**)	8.86×10^4	This work
$[(CH_3)_2NH_2]_6[Cd_3L(H_2O)_2]\cdot 12H_2O$	2.67×10^5	*ACS Appl. Mater. Interfaces.,* 2017, **9**, 39441-39449
$[Cd_2(pbdc)(H_2O)_3]$	1.86×10^5	*Cryst. Growth Des. 2018,* ***18****, 7683-7689*
$[Zn_3(L)_2(bipy)(\mu_3\text{-}OH)_2]$	2.3×10^4	*Sens Actuators B Chem.2018,* ***257****, 207-213*
Eu3+@Zn-MOF	1.9×10^4	*Inorg. Chem. 2017,* ***56****, 12348-12356*
$\{[Cd(TZMB)(DMA)]\cdot(H_2O)_{0.5}\}_n$	4.34×10^4	*CrystEngComm,* 2019, **21**, 5767-5778

ICP measurements:

After luminescence experiment, the suspension was filtered. Then, ICP measurements were performed on the filtrate (solution containing Fe^{3+} ions), the results are as following (Table S3).

Table S3. The concentration of Fe^{3+} and Cd^{2+} ($mol \cdot L^{-1}$)

MOF	1	2
The initial concentration of Fe^{3+}	1.0×10^{-3}	1.0×10^{-3}
The initial concentration of Cd^{2+}	—	—
The concentration of Fe^{3+} in filtrate after sensing measurement	0.7912×10^{-3}	0.9984×10^{-3}
The concentration of Cd^{2+} in filtrate after sensing measurement	—	—

Table S4. Crystal data for **1** and **2.**

MOF	1	2
Empirical formula	$C_{80}H_{50}Cd_4N_{10}O_{22}$	$C_{35}H_{22}Cd_2N_4O_{11}$
Formula weight	1952.94	899.39
Temperature/K	296.15	150.15
Crystal system	triclinic	monoclinic
Space group	*P-1*	$P2_1/c$
a/Å	14.865(2)	11.6552(4)
b/Å	15.836(3)	14.9367(7)
c/Å	19.119(3)	19.7696(8)
α/°	84.748(4)	90
β/°	89.922(4)	102.3140(10)
γ/°	87.094(4)	90
Volume/$Å^3$	4476.0(13)	3362.5(2)
Z	2	4
ρ_{calcg}/cm^3	1.449	1.777
μ/mm^{-1}	1.009	1.334
F(000)	1936.0	1776.0
Radiation	MoKα (λ = 0.71073)	MoKα (λ = 0.71073)
2θ range (deg)	2.14 to 50.054	4.498 to 52.856
Data/restraints/parameters	15712/0/1049	6882/132/507
Gof	1.031	1.147
R_1, wR_2 (I>=2σ (I))[a,b]	0.0675, 0.1607	0.0430, 0.0834
R_1, wR_2 (all data)	0.1267, 0.1870	0.0536, 0.0865
CCDC number	1956741	1956743

[a] $R_1 = \Sigma| |F_o|-|F_c| | / \Sigma|F_o|$, $wR_2 = [\Sigma w(F_o^2-F_c^2)^2] / \Sigma w(F_o^2)^2]^{1/2}$

Table S5. Selected bond lengths (Å) and angles (deg) for MOF **1**

Cd1-O3	2.227(7)	O3-Cd1-O3^1	78.4(3)	O17^4-Cd3-O8	103.0(3)	O12-Cd4-O11^7	79.2(2)
Cd1-O3^1	2.289(6)	O3-Cd1-O9^2	113.5(2)	O17^4-Cd3-O16^4	98.1(2)	O12-Cd4-O16^7	100.1(2)
Cd1-O9^2	2.351(6)	O3^1-Cd1-O9^2	113.7(2)	O17^4-Cd3-O18	167.9(3)	O12-Cd4-C16^6	108.5(3)
Cd1-O10^2	2.306(6)	O3^1-Cd1-O10^2	165.7(2)	O18-Cd3-O16^4	78.4(2)	O12-Cd4-C45^7	90.5(2)
Cd1-O19^1	2.277(7)	O3-Cd1-O10^2	114.3(3)	N4-Cd3-O8	99.5(3)	O15^7-Cd4-Cd4^7	75.65(16)
Cd1-O20^1	2.443(6)	O3-Cd1-O19^1	139.3(2)	N4-Cd3-O16^4	83.3(3)	O15^7-Cd4-O2^6	78.3(2)
Cd2-N6	2.247(7)	O3^1-Cd1-O20^1	87.2(2)	N4-Cd3-O17^4	100.5(2)	O15^7-Cd4-O11^7	79.7(2)
Cd2-O4	2.401(6)	O3-Cd1-O20^1	85.6(2)	N4-Cd3-O18	90.6(2)	O15^7-Cd4-O12	152.1(2)
Cd2-O5	2.247(6)	O9^2-Cd1-O20^1	153.5(3)	N4-Cd3-N9^5	175.5(3)	O15^7-Cd4-O16^7	81.1(2)
Cd2-O6^3	2.304(6)	O10^2-Cd1-O9^2	56.2(2)	N9^5-Cd3-O8	81.4(3)	O11-Cd4-O16^7	139.2(2)
Cd2-O7	2.443(7)	O10^2-Cd1-O20^1	99.9(2)	N9^5-Cd3-O16^4	94.2(3)	O12-Cd4-O2^6	125.3(2)
Cd2-N1	2.282(8)	O19^1-Cd1-O3^1	88.0(2)	N9^5-Cd3-O17^4	83.6(3)	O11-Cd4-O12	81.5(2)
Cd3-O8	2.333(8)	O19^1-Cd1-O9^2	107.1(2)	N9^5-Cd3-O18	85.1(3)	O11-Cd4-O15^7	79.9(2)
Cd3-O16^4	2.464(7)	O19^1-Cd1-O10^2	85.9(3)	O8-Cd3-O16^4	157.7(2)	O11^7-Cd4-O16^7	52.7(2)
Cd3-O17^4	2.306(6)	O19^1-Cd1-O20^1	55.3(2)	O8-Cd3-O18	79.5(3)	N6-Cd2-O4	85.3(2)
Cd3-O18	2.416(6)	O4-Cd2-O7	75.2(2)	O1^6-Cd4-O2^6	54.9(3)	N6-Cd2-O5	101.7(3)
Cd3-N4	2.218(7)	O5-Cd2-O4	98.5(2)	O1^6-Cd4-O11^7	132.0(2)	N6-Cd2-O6^3	89.3(2)
Cd3-N9^5	2.226(8)	O5-Cd2-O6^3	102.5(2)	O1^6-Cd4-O12	85.8(2)	N6-Cd2-O7	84.8(3)

Cd4-O16^{6}	2.471(6)	O5-Cd2-O7	170.7(2)	O1^{6}-Cd4-O15^{7}	122.0(2)	N6-Cd2-N1	170.7(3)
Cd4-O1^{7}	2.308(7)	O5-Cd2-N1	85.6(3)	O1^{6}-Cd4-O16^{7}	86.3(2)		
Cd4-O2^{7}	2.413(7)	O6^{3}-Cd2-O4	158.9(2)	O2^{6}-Cd4-O11^{7}	155.1(2)		
Cd4-O11	2.304(7)	O63-Cd2-O7	84.0(2)	O2^{6}-Cd4-O167	112.0(2)		
Cd4-O11^{6}	2.416(6)	N1-Cd2-O4	99.4(3)	O11-Cd4-O16	134.2(2)		
Cd4-O12	2.329(5)	N1-Cd2-O6^{3}	83.4(3)	O11-Cd4-O2^{6}	99.1(3)		
Cd4-O15^{6}	2.314(5)	N1-Cd2-O7	88.6(3)	O11-Cd4-O11^{7}	88.4(2)		

Symmetry codes: (1) 1-x, -y, 1-z; (2) x, -1+y, z; (3) -x, -y, 1-z; (4) 1-x, 2-y, -z; (5) x, 2+y, -1+z; (6) 2-x, 2-y, -z; (7) 1+x, 1+y, z; (8) -1+x, -1+y, z; (9) x, 1+y, z; (10) x, -2+y, 1+z

Table S6. Selected bond lengths (Å) and angles (deg) for MOF **2**

Cd1-O1^{1}	2.318(3)	O1^{1}-Cd1-O1	75.90(11)	O5^{3}-Cd1-O1	135.58(12)	O11-Cd2-O2	80.70(13)
Cd1-O1	2.356(3)	O1-Cd1-O2	53.90(10)	O5^{3}-Cd1-O2	81.97(12)	N3^{5}-Cd2-O11	87.26(14)
Cd1-O2	2.499(3)	O1^{1}-Cd1-O2	124.23(10)	O5^{3}-Cd1-O7	93.34(12)	N1-Cd2-O2	89.11(13)
Cd1-O5^{2}	2.233(3)	O1-Cd1-O7	78.48(11)	O5^{3}-Cd1-O9^{2}	82.62(12)	N1-Cd2-O3	99.70(14)
Cd1-O7	2.477(3)	O1^{1}-Cd1-O7	76.67(11)	O5^{3}-Cd1-O10^{2}	81.87(13)	N1-Cd2-O4^{4}	94.26(14)
Cd1-O9^{3}	2.348(3)	O1^{1}-Cd1-O9^{2}	92.48(11)	O7-Cd1-O2	71.44(10)	N1-Cd2-O11	88.41(14)
Cd1-O10^{3}	2.423(3)	O1-Cd1-O10^{2}	83.59(11)	O9^{2}-Cd1-O1	121.23(11)	N1-Cd2-N3^{5}	175.64(15)
Cd2-O2	2.419(3)	O1^{1}-Cd1-O10^{2}	123.23(12)	O9^{2}-Cd1-O2	131.76(11)	N3^{5}-Cd2-O2	90.70(13)
Cd2-O3	2.310(3)	O5^{3}-Cd1-O1^{1}	145.00(12)	O3-Cd2-O2	101.83(11)	N3^{5}-Cd2-O3	84.60(13)
Cd2-O4^{4}	2.309(3)	O9^{2}-Cd1-O10^{2}	55.26(12)	O3-Cd2-O11	171.50(13)	N3^{5}-Cd2-O4^{4}	84.63(14)
Cd2-O11	2.401(4)	O10^{2}-Cd1-O2	77.42(11)	O4^{4}-Cd2-O2	162.41(11)		
Cd2-N1	2.243(4)	O10^{2}-Cd1-O7	148.85(12)	O4^{4}-Cd2-O3	94.63(12)		
Cd2-N3^{5}	2.253(4)	O9^{2}-Cd1-O7	154.93(11)	O4^{4}-Cd2-O11	82.14(14)		

Symmetry codes: (1) 2-x, 1-y, 2-z; (2) x, 1.5-y, -0.5+z; (3) 1+x, y, z; (4) 2-x, 2-y, 2-z; (5) 1+x, 1.5-y, 0.5+z; (6) x, 1.5-y, 0.5+z; (7) -1+x, y, z; (8) -1+x, 1.5-y, -0.5+z.**).**